Coupled Systems Mechanics, *Vol. 14, No. 2 (2025) 175-199*
https://doi.org/10.12989/csm.2025.14.2.175

Combined effects of partial loading and partial elastic foundation on the bending response of functionally graded structures

Abderrahmane Menasria[1,3a], Nabil Himeur[2,4a], Abdelhakim Bouhadra*[1,3], Messaoud Bazzouzi[1,5a] and Abdelouahed Tounsi[4,5a]

[1]*Civil Engineering Department, Faculty of Sciences and Technology, University of Khenchela, BP 1252 Road of Batna, Khenchela 40000, Algeria*
[2]*Mechanical Engineering Department, Faculty of Sciences and Technology, University of Khenchela, BP 1252 Road of Batna, Khenchela 40000, Algeria*
[3]*Materials and Hydrology Laboratory, University of Sidi Bel Abbes, BP 89, Sidi Bel Abbes, 22000, Algeria*
[4]*Laboratory of Engineering and Sciences of Advanced Materials, BP 1252 Road of Batna, Khenchela 40000, Algeria*
[5]*Laboratory of Research in Civil Engineering (LRGC), University of Biskra, BP14507000 Biskra, Algeria*
[6]*Department of Civil and Environmental Engineering, King Fahd University of Petroleum & Minerals, 31261 Dhahran, Eastern Province, Saudi Arabia*

(Received February 17, 2025, Revised May 21, 2025, Accepted May 23, 2025)

Abstract. This study uniquely investigates functionally graded nanoplates under combined partial loading and non-uniform elastic support, developing a quasi-3D model, a unified analytical framework for complex foundations, and novel closed-form solutions, thereby addressing a critical yet underexplored area in structural mechanics. A simplified quasi-3D high-order shear deformation theory incorporating integral terms is used. The governing equilibrium equations consider the interaction between the loading type and the variation of Winkler-Pasternak and Kerr foundation parameters. The numerical results for non-dimensional stresses and displacements are obtained using the virtual displacement principle and Navier's solution technique. The accuracy of the non-dimensional formulas is validated against existing literature, demonstrating excellent agreement. Additionally, several parametric studies examine the effects of various geometric and material factors. This analytical model is well suited for analyzing the bending behaviour of simply supported FG plates in specific engineering applications.

Keywords: elastic bending; FG nanoplates; Navier solution; partial foundation; partial loads; quasi-3D theory

1. Introduction

Functionally graded materials are materials whose mechanical properties vary continuously

*Corresponding author, Professor, E-mail: bouhadrahako@gmail.com
[a]Ph.D.

http://www.techno-press.org/?journal=csm&subpage=8 ISSN: 2234-2184 (Print), 2234-2192 (Online)

with position, and the material properties are graded in composition to optimize the materials for a desired application. Because the ability can have different mechanical properties based on their position in the material, they are advantageous in structural materials where optimal mechanical behavior is desired. FGMs have been widely used in mechanical design, thermal barrier coatings, biomedical applications, and non-toxic materials in nuclear support applications. The behavior and characteristics of FGMs are based on the following criteria: the production techniques used to produce the materials through different existing materials, the behavior of the layering and its influence on the mechanical response and performance of the FGM, the fracturing of FGM materials and how the features of the material combinations mitigate the failure, and the factor of modeling and numerical work that are employed in the work.

The integration of functional gradient materials (FGMs) into the design of various structural components has become essential in nanotechnology because of their unique properties and benefits of these advanced materials, which address the limitations of traditional composite materials. Nanoplates crafted from functionally graded materials often experience combined stresses in their intended environments.

Functionally Graded Materials (FGMs) are increasingly utilized in diverse structural applications across civil and mechanical engineering owing to their tailored properties that vary gradually over the volume. These materials are particularly advantageous in scenarios involving partial loading and support, where traditional homogeneous materials may not perform well. Examples include pavements and roadways subjected to various types of loading and resting on layered subgrades, where different soil layers interact through shear and compression, as well as rail tracks supported by sleepers and ballast, considering both vertical and shear interactions with the subgrade. This is also applicable to Functionally Graded Material (FGM) plates and composite panels in aerospace and marine structures, where the foundation represents elastic layers or underlying support materials. It is also used in bridges, viaducts, machine foundations, and buried pipelines and tunnels.

Various analytical methods have been employed in the aforementioned engineering fields to evaluate the bending behavior of these components. Slimani *et al.* (2024) investigated a quasi-three-dimensional (3D) refinement employing a novel higher-order shear deformation theory to assess static bending with two types of porous porosity distribution. Khadraoui *et al.* (2022) explored the impact of thickness stretching and nonlinear hygro-thermo-mechanical loading on the bending behaviour of functionally graded (FG) beams. The Young's modulus, thermal expansion, and moisture concentration coefficients were assumed to vary gradually and continuously according to a power-law distribution with respect to the volume fractions of the constituent materials. Furthermore, the governing equilibrium equations considered the interactions between the thermal, mechanical, and moisture loads. Meski *et al.* (2024) conducted a study on the nonlinear hygro-thermo-mechanical coupling loading (NL-HTMCL) of functionally graded sandwich beams (FGSBs). This study considered various symmetric and nonsymmetric beam configurations with FGSB skins. A novel quasi-three-dimensional (quasi-3D) high shear deformation theory was employed to analyze the behavior of these multi-type sandwich beams. Li *et al.* (2024) developed analytical expressions for the bending solutions of a simply supported rectangular functionally graded material (FGM) plate using a four-variable refined higher-order shear deformation theory. These solutions were directly related to the corresponding solutions of a homogeneous Kirchhoff plate under the classical plate theory. The deflection, stress components, resultant forces, and bending moments of the thick FGM plate were analytically expressed in terms of the deflection of a reference homogeneous Kirchhoff plate with identical geometry,

loadings, and boundary conditions. Kahya and Turan (2017) examined the bending response of a composite laminate beam under different boundary conditions using higher-order beam theory. Kahya and Turan (2018) studied the stability and dynamic behavior of a multi-layered composite beam with different edges using a higher-order layer-wise theory. The element matrices for the single- and multilayer beam elements were obtained using Lagrange's equations. Turan and Kahya (2021) investigated the dynamic and stability behaviors of two types of FG sandwich beams using the FSDBT. The volumetric ceramic ratio was defined as a force function. The governing equations of motion were obtained using the Lagrange principle. The Navier solution technique was used for different boundary conditions. Turan (2022) studied the bending response of Bi-directional FG beams based on the first-order shear deformation beam theory. The material properties of the beam were defined using a power-law rule. The equilibrium equations were derived using the Lagrange principle. A Navier-type solution for different boundary conditions represented by trigonometric series functions was used to solve the problem and obtain the transverse deflections, axial shear stresses, and transverse shear stresses. Turan and Adiyaman (2023) examined the bending behavior of imperfect bi-directional FG beams using a new higher-order finite element and a new sinusoidal uneven distribution function. The governing equilibrium equations are obtained using Lagrange's principle. Turan *et al.* (2023) investigates the dynamic and the stability response of imperfect FG beams with bi-directional distributions of ceramic volume fraction using an analytical solution based on the first-order shear deformation theory, finite element (FEM) and artificial neural network (ANN) methods. Turan and Adiyaman (2024) investigated the dynamic and stability responses of imperfect bidirectional functionally graded beams with various boundary conditions. The material gradation across both directions was defined using a power-law function. The governing equations of motion were derived using Lagrange's principle. Turan (2024) presented a new analytical solution using the Ritz method to examine the dynamic and stability behaviors of imperfect bi-directional functionally graded beams with different boundary edges. The solution employs first-order shear deformation theory (FSDT) and utilizes mixed series functions combining polynomial and trigonometric expressions tailored to each boundary edge. The equations of motion are derived using Lagrange's principle, accounting for the power-law variation of the material components throughout the beam's volume. Adiyaman and Turan (2025) examined the equilibrium and stability of imperfect bidirectional functionally graded beams using higher-order shear deformation theory. Exponential functions were used to show the material property disparities, and three porosity distribution functions were considered. The governing equations were derived using Lagrange's principle, and a finite element model with two nodes and eight degrees of freedom was employed for the numerical analysis. Turan (2025) presented a first shear-deformable finite element model for the bending response of functionally graded beams with two-directional power-law distributions. The model incorporates ten degrees of freedom across five nodes, perfectly capturing the axial and shear deformations. A novel approach combines finite element analysis with Artificial Neural Network (ANN) methods to investigate the static behavior of BD-FGBs. Additional researchers have restricted their attention to many bending structures (Houari *et al.* 2003, Yushan and Zhen 2024, Huang *et al* 2023, Chitour *et al.* 2022).

Foroutan and Dai (2024) investigated the nonlinear dynamic behavior of both free and forced vibrations of thin, oblique shallow shells reinforced with stiffeners, possessing porosity, and made of functionally graded (FG) materials. The shells were assumed to be embedded in a nonlinear elastic foundation. He and She (2024) investigated the nonlinear forced vibrations of imperfect functionally graded (FG) beams exposed to hygrothermal coupled effects. The imperfections in the

beam can be attributed to manufacturing defects, material inconsistencies, or geometric irregularities. Chen *et al.* (2024), investigates the vibration response of bi-directional FG sandwich beams laying on an elastic foundation, using the FSDBT of Timoshenko, which accounts for both bending and shear deformations. Najafi *et al.* (2024) presents a novel three-dimensional displacement-based formulation accounting for stretching effect of functionally graded nanoplates. The mechanical properties of the nanoplates vary gradually in the *z*-direction of the plate according to a power-law distribution. The model does not assume a predetermined form for the distribution of displacements and transverse strains, distinguishing it from traditional shear deformation theory. The governing equations of motion were obtained based on the Hamilton principle and resolved for simply supported nanoplates. Abdelrahman *et al.* (2024) examines the dynamic response of FG beams, which have cracks and are laying on a Winkler elastic foundation when subjected to moving loads. The obtained numerical results show how the presence of cracks, material gradation, and characteristics of the elastic foundation affect the dynamic response of beams under moving loads. Eghbali and Hosseini (2024) developed a precise analytical model to examine the vibration behaviour of Carbon Nanotube Reinforced Composite (CNTRC) beams subjected to both harmonic and constant loads. These beams are supported by a Pasternak-type elastic foundation, which accounts for both normal and shear interactions between the beam and foundation. Shen *et al.* (2024) investigated the free vibration response of spherical cap shells made of imperfect functionally graded materials reinforced with graphene platelets (GPLs) and laid on a Winkler elastic foundation. Mohammed *et al.* (2024) developed a semi-analytical model to study the free vibration characteristics of cylindrical shells with a damaged core, laminated with FG carbon nanotube-reinforced composite (FG-CNTRC) face sheets, and supported on a two-parameter elastic foundation. Fan and She (2025) investigated the dynamic response of beams composed of graphene platelets reinforced metal foams (GPLRMFs) under transient loading conditions, incorporating the effects of initial geometric imperfections and viscoelastic foundations. She *et al.* (2024) explored the thermal stability and post-buckling behavior of beams made from graphene platelets reinforced metal foams (GPLRMFs), considering the influence of initial geometric imperfections.

Elastic foundation-supported plates are widely used in various structural applications, including aircraft runways, deep wells, bridges, and buildings, among others. The simplest model for such foundations is the Winkler model (Wu *et al.* 2011), which represents the foundation as a series of independent springs without interaction. Pasternak extended the Winkler model by introducing a shear layer between the springs, resulting in a two-parameter model. This approach is also known as the Pasternak foundation model (Yaghoobi & Fereidoon, 2014). Do *et al.* (2024) conducted a nonlinear static bending analysis of functionally graded porous sandwich plates with a ceramic core (FSCC). The FSCC plates were assumed to rest on a Kerr foundation and subjected to a transverse uniform load. The analysis utilized the mixed interpolation of tensorial components for a four-node rectangular element (MITC4). Kumar *et al.* (2024) developed an analytical solution for the bending analysis of functionally graded porous sandwich plates with and without holes supported by elastic foundations. The analysis employed first-order shear deformation theory within a finite element method framework. Hoang *et al.* (2023) developed a novel theoretical model to analyze the effects of an arbitrarily distributed Kerr foundation on the free vibration and transient responses of functionally graded material plates in a thermal environment. The mechanical properties of the FGM plates were assumed to vary with the plate thickness according to a power-law distribution. The three-parameter Kerr model is based on the independence of the upper and lower elastic layers from the shear layer. The shape and location of the elastic

foundation were defined arbitrarily using mathematical function. Tamrabet *et al.* (2023) investigated the influence of porosity on the buckling behaviour of thick functionally graded sandwich plates. The plates were subjected to various in-plane loads and supported under different boundary conditions. A newly developed sandwich plate theory incorporating a modified power-law function for symmetric and asymmetric configurations was used in the formulation. Other exciting studies have focused on the bending analysis of composite structures supported by various types of elastic foundations (Chitour *et al.* 2022, Hoang *et al.* 2024, Soltani *et al* 2024, Salehipour *et al.* 2024, Rachid *et al.* 2022, Han and Liew 1997, Thai *et al.* 2013, Nebab *et al.* 2019, Park and Choi 2018, Zenkour *et al.* 2014, Ameur *et al.* 2011).

This study investigates the coupled influence of variable Winkler-Pasternak and Kerr foundations on the bending behavior of functionally graded (FG) plates. The key objective of this study was to examine the plate response under various loading conditions. Himeur *et al.* (2022) proposed a novel quasi-3D theory to analyze the coupled effects of variable Winkler-Pasternak foundations on functionally graded (FG) plates. The theory considers the simultaneous variation of both parameters of the Winkler-Pasternak foundation while the FG plates are subjected to different loading conditions.

The originality of this study lies in its innovative examination of functionally graded (FG) plates subjected to concurrent partial loading and nonuniform foundation support, a critical configuration that has been largely overlooked in the existing literature. Our research contributes significantly to three key areas: the development of a comprehensive quasi-3D model that accurately captures the through-thickness stress distributions under partial loading conditions, the formulation of a unified analytical framework that incorporates partial Winkler-Pasternak and Kerr foundations, and the derivation of novel closed-form solutions for partially elastic foundations on FG plates under various loading scenarios. These advancements substantially enhance the accuracy of predictions for practical engineering applications in which structures encounter localized loads while being partially supported, such as in industrial flooring, foundation engineering, and advanced composite structures in aerospace and civil infrastructure applications. This quasi-3D theory, using integral terms, investigates the effects of variable Winkler-Pasternak and Kerr foundations on the bending behavior of functionally graded (FG) plates under various loading conditions. The Navier solution technique, which employs a double Fourier series and satisfies the boundary conditions of a simply supported plate, was used to solve the resulting equilibrium equations. This study considers the effects of thickness stretching, power-law index, side-to-thickness ratio, plate aspect ratio, load type, and Winkler-Pasternak and Kerr foundation parameters on the bending behavior.

2. Mathematic formulation

A simply supported FGM plate of length a, width b, and thickness h, resting on an elastic foundation. The x, y, and z coordinates were taken according to the length, width, and thickness, respectively, as shown in Fig. 1. Otherwise, the material properties vary smoothly and continuously across the thickness of FGM face sheets.

The Voigt mixing rule can express the effective properties of the material, such as Young's modulus E, Poisson's ratio υ, and mass density ρ, which are described mathematically according to the relationships given in reference Slimani *et al.* (2024).

$$P(z) = P_m + (P_c - P_m)V_c \tag{1}$$

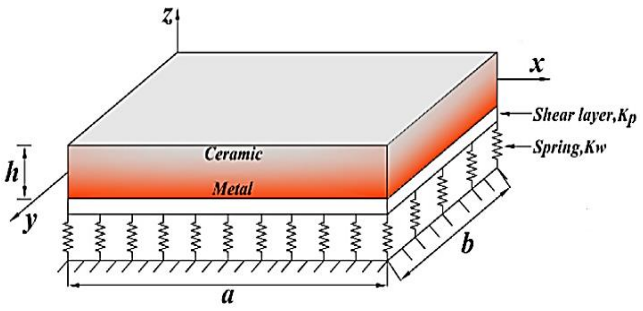

(a)

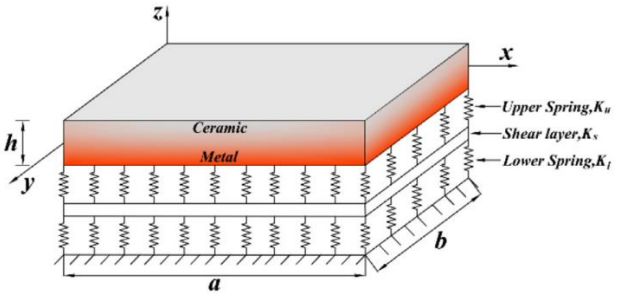

(b)

Fig. 1 The geometry of rectangular FGM plate resting on (a) Winkler-Pasternak foundation and (b) Kerr foundation

where P_c and P_m represent the properties of the ceramic and metal materials, respectively, and (V_c) represents the volume fraction of the ceramic.

$$V_c = \left(\frac{1}{2} + \frac{z}{h}\right)^k \tag{2}$$

Based on the thick plate integral model and fulfilling the transverse shear stresses and deformation requirements, which disappear at the upper and lower sides of the plate ($z=\pm h/2$), the following displacement field of the plate can be used as Zaoui *et al.* (2019)

$$\begin{aligned} u(x,y,z) &= u_0(x,y) - z\frac{\partial w_0}{\partial x} + k_1 f(z)\int \theta(x,y)\,dx \\ v(x,y,z) &= v_0(x,y) - z\frac{\partial w_0}{\partial y} + k_2 f(z)\int \theta(x,y)\,dy \\ w(x,y,z) &= w_0(x,y) + g(z)\phi_z(x,y) \end{aligned} \tag{3}$$

Where: u_0, v_0, w_0, θ and ϕ_z are defined as the median plane, five unknown displacements of the plate. The coefficient $k_1 = \alpha^2$ and $k_2 = \beta^2$ are related to the plate's geometry. The displacement field implies only five unknowns when considering the thickness-stretching effect.

The shape function $f(z)$ and its derivative function $g(z)$ are presented in the following

$$f(z) = \frac{3\pi z}{25}\left[\pi - \sqrt[3]{0.135}\cosh\left(\frac{\pi z}{h}\right)\right]$$

and

$$g(z) = \frac{3\pi^2}{25} - \frac{3\pi^2\sqrt[3]{0.135}}{25}\cosh\left(\frac{\pi z}{h}\right) - \frac{3\pi^3 z\sqrt[3]{0.135}}{25}\sin h\left(\frac{\pi z}{h}\right) \tag{4}$$

The relationships between strains and displacements, established from the displacements field, are expressed under the following compact form

$$\begin{Bmatrix}\varepsilon_x\\ \varepsilon_y\\ \gamma_{xy}\end{Bmatrix}=\begin{Bmatrix}\varepsilon_x^0\\ \varepsilon_y^0\\ \gamma_{xy}^0\end{Bmatrix}+z\begin{Bmatrix}k_x^b\\ k_y^b\\ k_{xy}^b\end{Bmatrix}+f(z)\begin{Bmatrix}k_x^s\\ k_y^s\\ k_{xy}^s\end{Bmatrix},$$
$$\begin{Bmatrix}\gamma_{yz}\\ \gamma_{xz}\end{Bmatrix}=f'(z)\begin{Bmatrix}\gamma_{yz}^0\\ \gamma_{xz}^0\end{Bmatrix}+g(z)\begin{Bmatrix}\gamma_{yz}^1\\ \gamma_{xz}^1\end{Bmatrix}, \tag{5}$$
$$\varepsilon_z=g'(z)\,\varepsilon_z^0$$

Where

$$\begin{Bmatrix}\varepsilon_x^0\\ \varepsilon_y^0\\ \gamma_{xy}^0\end{Bmatrix}=\begin{Bmatrix}\frac{\partial u_0}{\partial x}\\ \frac{\partial v_0}{\partial y}\\ \frac{\partial u_0}{\partial y}+\frac{\partial v_0}{\partial x}\end{Bmatrix},\begin{Bmatrix}k_x^b\\ k_y^b\\ k_{xy}^b\end{Bmatrix}=\begin{Bmatrix}-\frac{\partial^2 w_0}{\partial x^2}\\ -\frac{\partial^2 w_0}{\partial y^2}\\ -2\frac{\partial^2 w_0}{\partial x\partial y}\end{Bmatrix} \tag{6}$$

$$\begin{Bmatrix}k_x^s\\ k_y^s\\ k_{xy}^s\end{Bmatrix}=\begin{Bmatrix}k_1\theta\\ k_2\theta\\ k_1\frac{\partial}{\partial y}\int\theta\,dx+k_2\frac{\partial}{\partial x}\int\theta\,dy\end{Bmatrix},$$
$$\begin{Bmatrix}\gamma_{yz}^0\\ \gamma_{xz}^0\end{Bmatrix}=\begin{Bmatrix}k_2\int\theta\,dy\\ k_1\int\theta\,dx\end{Bmatrix},\varepsilon_z^0=\phi_z \tag{7}$$

The terms written as integral in the previous formulation are resolved by the Navier method and might be given as indicated

$$\frac{\partial}{\partial y}\int\theta\,dx=A'\frac{\partial^2\theta}{\partial x\partial y},\frac{\partial}{\partial x}\int\theta\,dy=B'\frac{\partial^2\theta}{\partial x\partial y} \tag{8}$$

The coefficients A' and B' are written based on the Navier solution. Therefore, A', B', k_1 and k_2 as follows

$$A'=-\frac{1}{\alpha^2},B'=-\frac{1}{\beta^2},k_1=\alpha^2,k_2=\beta^2 \tag{9}$$

Where α and β are defined by

$$\alpha=m\pi/a \text{ and } \beta=n\pi/b \tag{10}$$

2.1 Constitutive relations

According to the nonlocal elasticity theory developed by Eringen (1983) and Eringen and Edelen (1972), the nonlocal constitutive relations of an FG sandwich nanoplate can be written as

$$(1-\nabla^2\mu^2)\begin{Bmatrix}\sigma_{xx}\\ \sigma_{yy}\\ \sigma_{zz}\\ \tau_{xz}\\ \tau_{yz}\\ \tau_{xy}\end{Bmatrix}^{(n)}=\begin{bmatrix}C_{11}&C_{12}&C_{13}&0&0&0\\ C_{12}&C_{22}&C_{23}&0&0&0\\ C_{13}&C_{23}&C_{33}&0&0&0\\ 0&0&0&C_{44}&0&0\\ 0&0&0&0&C_{55}&0\\ 0&0&0&0&0&C_{66}\end{bmatrix}^{(n)}\begin{Bmatrix}\varepsilon_{xx}\\ \varepsilon_{yy}\\ \varepsilon_{zz}\\ \gamma_{xz}\\ \gamma_{yz}\\ \gamma_{xy}\end{Bmatrix}^{(n)} \tag{11}$$

Where $\mu = e_0\ell$ represents a nonlocal coefficient that reveals the effects of small scales in nanostructures. In this case, ℓ denotes an internal characteristic length while e_0 does Eringen's present a constant Eringen (1983) as follows

$$e_0 = \frac{\sqrt{\pi^2-4}}{2\pi} \tag{12}$$

2.2 Equations of equilibrium

The theory of virtual displacements is used to determine the governing equations of the equilibrium state. In the instant case, the principle of virtual is expressed as

$$\int_V \delta U + \delta V + \delta U_R = 0 \tag{13}$$

Where δU,δV and δU_R are the variations in the strain energy, potential energy of the applied loads, and potential energy of the foundation, respectively.

The strain energy variation of the FG plate is obtained by

$$\begin{aligned}\delta U = \int_A [N_x\delta\varepsilon_x^0 + N_y\delta\varepsilon_y^0 + N_z\delta\varepsilon_z^0 + N_{xy}\delta\gamma_{xy}^0 + M_x^b\delta k_x^b + M_y^b\delta k_y^b + M_{xy}^b\delta k_{xy}^b \\ + M_x^s\delta k_x^s + M_y^s\delta k_y^s + M_{xy}^s\delta k_{xy}^s + S_{yz}^S\delta\gamma_{yz} + S_{xz}^S\delta\gamma_{xz}]dA = 0\end{aligned} \tag{14}$$

where A represents the plane section, and N, M, Q, and S are, respectively, in-plane force resultants, moment resultants, and transverse shear stress resultants; the following formulas determine all of those

$$\begin{Bmatrix} N_x & N_y & N_{xy} \\ M_x^b & M_y^b & M_{xy}^b \\ M_x^s & M_y^s & M_{xy}^s \end{Bmatrix} = \int_{-h/2}^{h/2} (\sigma_x, \sigma_y, \tau_{xy}) \begin{Bmatrix} 1 \\ z \\ f(z) \end{Bmatrix} dz \tag{15a}$$

$$N_z = \int_{-h/2}^{h/2} \sigma_z \ \mathrm{g}'(z)\ dz \tag{15b}$$

$$(S_{xz}^s, S_{yz}^s) = \int_{-h/2}^{h/2} (\tau_{xz}, \tau_{yz})\ \mathrm{g}(z)\ dz \tag{15c}$$

The expression of the variation of the applied load potential energy can be written as

$$\delta V = -\int_A q\delta\,(w_0(x,y) + g(z)\phi_z(x,y))dA \tag{16}$$

Also, elastic foundation potential energy variation can be annotated as

$$\delta U_R = \int f_e^{Pasternak,ker\,r}\,\delta w dA \tag{17}$$

f_e is the density of the reaction force generated by the foundation. For the Pasternak foundation model, it is given as follows

$$f_e^{Pasternak} = K_w w - K_g\nabla^2 w \tag{18a}$$

Here, K_w is the Winkler parameter, K_g is the shear layer foundation stiffness, ∇^2 is the Laplace operator in x and y, and w is the plate deflection.

The distributed reaction of the Kerr foundation model is defined as follows: Mekerbi *et al.* (2021)

$$f_e^{kerr} = \left(\frac{k_l k_u}{k_l + k_u}\right) w - \left(\frac{k_s k_u}{k_s + k_u}\right) \nabla^2 w \tag{18b}$$

By replacing the formulation of δU, δV and δU_R in the Eq. (13)

$$\begin{gathered} \int_V \delta U + \delta V + \delta U_R = \int_A [N_x \delta\varepsilon_x^0 + N_y \delta\varepsilon_y^0 + N_z \delta\varepsilon_z^0 + N_{xy} \delta\gamma_{xy}^0 \\ + M_x^b \delta k_x^b + M_y^b \delta k_y^b + M_{xy}^b \delta k_{xy}^b + M_x^s \delta k_x^s + M_y^s \delta k_y^s + M_{xy}^s \delta k_{xy}^s \\ + Q_{yz}^S \delta\gamma_{yz}^0 + S_{yz}^S \delta\gamma_{yz}^1 + Q_{xz}^S \delta\gamma_{xz}^0 + S_{xz}^S \delta\gamma_{xz}^1] dA \\ - \int_A q \delta w_0 dA - \int_A q g(z) \delta\phi_z dA + \int_A R \delta w_0 dA + \int_A R g(z) \delta\phi_z dA = 0 \end{gathered} \tag{19}$$

The five equations of equilibrium state in the current case are reached by integration by parts and collecting the unknowns' displacement $\delta u_0, \delta v_0, \delta w_0, \delta\theta$ and $\delta\phi_z$

$$\delta u_0: \quad \frac{\partial N_x}{\partial x} + \frac{\partial N_{xy}}{\partial y} = 0 \tag{20a}$$

$$\delta v_0: \quad \frac{\partial N_{xy}}{\partial x} + \frac{\partial N_y}{\partial y} = 0 \tag{20b}$$

$$\delta w_0: \quad \frac{\partial^2 M_x^b}{\partial x^2} + 2\frac{\partial^2 M_{xy}^b}{\partial x \partial y} + \frac{\partial^2 M_y^b}{\partial y^2} + q - R = 0 \tag{20c}$$

$$\delta\theta: \quad -k_1 M_x^s - k_2 M_y^s - (k_1 A' + k_2 B') \frac{\partial^2 M_{xy}^s}{\partial x \partial y} + \frac{\partial S_{xz}^s}{\partial x} + \frac{\partial S_{yz}^s}{\partial y} = 0 \tag{20d}$$

$$\delta\varphi_z: \quad \frac{\partial S_{xz}^s}{\partial x} + \frac{\partial S_{yz}^s}{\partial y} - N_z + g(z)(q - R) = 0 \tag{20e}$$

The in-plane force resultants N, moment resultants M, and the transverse shear stress resultant S are achieved as

$$\begin{gathered} \begin{Bmatrix} N \\ M^b \\ M^s \end{Bmatrix} = \begin{bmatrix} A & B & B^s \\ B & D & D^s \\ B^s & D^s & H^s \end{bmatrix} \begin{Bmatrix} \varepsilon \\ k^b \\ k^s \end{Bmatrix} + \begin{pmatrix} L \\ L^a \\ R \end{pmatrix} \varepsilon, \qquad S = A^s \gamma \\ N_z = R^a \varepsilon_z^0 + L(\varepsilon_x^0 + \varepsilon_y^0) + L^a (k_x^b + k_y^b) + R(k_x^s + k_y^s) \end{gathered} \tag{21}$$

Where

$$\begin{gathered} A = \begin{bmatrix} A_{11} & A_{12} & 0 \\ A_{12} & A_{22} & 0 \\ 0 & 0 & A_{66} \end{bmatrix}, \; B = \begin{bmatrix} B_{11} & B_{12} & 0 \\ B_{12} & B_{22} & 0 \\ 0 & 0 & B_{66} \end{bmatrix}, \\ D = \begin{bmatrix} D_{11} & D_{12} & 0 \\ D_{12} & D_{22} & 0 \\ 0 & 0 & D_{66} \end{bmatrix}, \; B^s = \begin{bmatrix} B_{11}^s & B_{12}^s & 0 \\ B_{12}^s & B_{22}^s & 0 \\ 0 & 0 & B_{66}^s \end{bmatrix}, \\ D^s = \begin{bmatrix} D_{11}^s & D_{12}^s & 0 \\ D_{12}^s & D_{22}^s & 0 \\ 0 & 0 & D_{66}^s \end{bmatrix}, \; \mathrm{H}^s = \begin{bmatrix} H_{11}^s & H_{12}^s & 0 \\ H_{12}^s & H_{22}^s & 0 \\ 0 & 0 & H_{66}^s \end{bmatrix} \end{gathered} \tag{22a}$$

$$\begin{Bmatrix} A_{11} & B_{11} & D_{11} & B_{11}^s & D_{11}^s & H_{11}^s \\ A_{12} & B_{12} & D_{12} & B_{12}^s & D_{12}^s & H_{12}^s \\ A_{66} & B_{66} & D_{66} & B_{66}^s & D_{66}^s & H_{66}^s \end{Bmatrix} = \int_{-h/2}^{h/2} \lambda(z) \begin{Bmatrix} 1 \\ z \\ z^2 \\ f(z) \\ zf(z) \\ f^2(z) \end{Bmatrix}^T \begin{Bmatrix} \frac{1-\nu}{\nu} \\ 1 \\ \frac{1-2\nu}{2\nu} \end{Bmatrix} dz \tag{22b}$$

$$\begin{Bmatrix} L \\ L^a \\ R \end{Bmatrix} = \int_{-h/2}^{h/2} C_{ij} \begin{Bmatrix} 1 \\ z \\ f(z) \end{Bmatrix} g'(z)\, dz, if\ (i = 1,2\ ;\ j = 3)$$
$$\{R^a\} = \int_{-h/2}^{h/2} C_{33}\ [g'(z)]^2 dz \tag{22c}$$

$$A^s = \begin{bmatrix} A_{44}^s & 0 \\ 0 & A_{55}^s \end{bmatrix}$$
$$A_{44}^s = A_{55}^s = \int_{-h/2}^{h/2} \left(\frac{E(z)}{2(1+v)}\ [g^2(z)]\right) dz \tag{22d}$$

$$(A_{22}, B_{22}, D_{22}, B_{22}^s, D_{22}^s, H_{22}^s) = (A_{11}, B_{11}, D_{11}, B_{11}^s, D_{11}^s, H_{11}^s) \tag{22e}$$

By replacing Eq. (21) into Eq. (20), the equation of equilibrium can be rewritten according to displacement terms (u_0, v_0, w_0, θ and ϕ) and the form of the equation becomes

$$\delta u_0 :\ A_{11}\frac{\partial^2 u_0}{\partial x^2} + A_{12}\frac{\partial^2 v_0}{\partial x \partial y} + A_{66}\left(\frac{\partial^2 u_0}{\partial y^2} + \frac{\partial^2 v_0}{\partial x \partial y}\right) - B_{11}\frac{\partial^3 w_0}{\partial x^3} - B_{12}\frac{\partial^3 w_0}{\partial x \partial y^2} - 2B_{66}\frac{\partial^3 w_0}{\partial x \partial y^2} + B_{11}^s k_1 \frac{\partial \theta}{\partial x} + B_{12}^s k_2 \frac{\partial \theta}{\partial x} + B_{66}^s (A' k_1 + B' k_2)\frac{\partial^3 \theta}{\partial x \partial y^2} + L\frac{\partial \varphi_z}{\partial x} = 0 \tag{23a}$$

$$\delta v_0 :\ A_{12}\frac{\partial^2 u_0}{\partial x \partial y} + A_{22}\frac{\partial^2 v_0}{\partial y^2} + A_{66}\left(\frac{\partial^2 u_0}{\partial x \partial y} + \frac{\partial^2 v_0}{\partial x^2}\right) - B_{12}\frac{\partial^3 w_0}{\partial x^2 \partial y} - B_{22}\frac{\partial^3 w_0}{\partial y^3} - 2B_{66}\frac{\partial^3 w_0}{\partial x^2 \partial y} + B_{12}^s k_1 \frac{\partial \theta}{\partial y} + B_{22}^s k_2 \frac{\partial \theta}{\partial y} + B_{66}^s (A' k_1 + B' k_2)\frac{\partial^3 \theta}{\partial x^2 \partial y} + L\frac{\partial \varphi_z}{\partial y} = 0 \tag{23b}$$

$$\delta w_0 : B_{11}\frac{\partial^3 u_0}{\partial x^3} + B_{12}\left(\frac{\partial^3 u_0}{\partial x \partial y^2} + \frac{\partial^3 v_0}{\partial x^2 \partial y}\right) + B_{22}\frac{\partial^3 v_0}{\partial y^3} + 2B_{66}\left(\frac{\partial^3 u_0}{\partial x \partial y^2} + \frac{\partial^3 v_0}{\partial x^2 \partial y}\right) - D_{11}\frac{\partial^4 w_0}{\partial x^4} - 2D_{12}\frac{\partial^4 w_0}{\partial x^2 \partial y^2} - D_{22}\frac{\partial^4 w_0}{\partial y^4} - 4D_{66}\frac{\partial^4 w_0}{\partial x^2 \partial y^2} + D_{11}^s k_1 \frac{\partial^2 \theta}{\partial x^2} + D_{12}^s\left(k_1 \frac{\partial^2 \theta}{\partial y^2} + k_2 \frac{\partial^2 \theta}{\partial x^2}\right) + D_{22}^s k_2 \frac{\partial^2 \theta}{\partial y^2} + 2D_{66}^s (A' k_1 + B' k_2)\theta \frac{\partial^4 \theta}{\partial x^2 \partial y^2} + L^a\left(\frac{\partial^2 \varphi_z}{\partial x^2} + \frac{\partial^2 \varphi_z}{\partial y^2}\right) + (1 - \mu^2 \nabla^2)(q - R) = 0 \tag{23c}$$

$$\delta\theta :\ -B_{11}^s k_1 \frac{\partial u_0}{\partial x} - B_{12}^s\left(k_1 \frac{\partial v_0}{\partial y} + k_2 \frac{\partial u_0}{\partial x}\right) - B_{22}^s k_2 \frac{\partial v_0}{\partial y} - B_{66}^s (A' k_1 + B' k_2)\left(\frac{\partial^3 u_0}{\partial x \partial y^2} + \frac{\partial^3 v_0}{\partial x^2 \partial y}\right) + D_{11}^s k_1 \frac{\partial^2 w_0}{\partial x^2} + D_{12}^s\left(k_1 \frac{\partial^2 w_0}{\partial y^2} + k_2 \frac{\partial^2 w_0}{\partial x^2}\right) + D_{22}^s k_2 \frac{\partial^2 w_0}{\partial y^2} + 2D_{66}^s (A' k_1 + B' k_2)\frac{\partial^4 w_0}{\partial x^2 \partial y^2} - H_{11}^s (k_1)^2 \theta - 2H_{12}^s k_1 k_2 \theta - H_{22}^s (k_2)^2 \theta - H_{66}^s (A' k_1 + B' k_2)^2 \frac{\partial^4 \theta}{\partial x^2 \partial y^2} + A_{55}^s (A' k_1)\frac{\partial^2 \theta}{\partial x^2} + A_{44}^s (B' k_2)\frac{\partial^2 \theta}{\partial y^2} + R(k_1 + k_2)\varphi_z + A_{55}^s A' k_1 \frac{\partial^2 \varphi_z}{\partial x^2} + A_{44}^s B' k_2 \frac{\partial^2 \varphi_z}{\partial y^2} = 0 \tag{23d}$$

$$\delta\varphi_z: -L(\frac{\partial u_0}{\partial x}+\frac{\partial v_0}{\partial y})+L^a(\frac{\partial^2 w_0}{\partial x^2}+\frac{\partial^2 w_0}{\partial y^2})+(k_2(A_{44}^s-R)+k_1(A_{55}^s-R))\theta-R^a\varphi_z+ A_{55}^s\frac{\partial^2\varphi_z}{\partial x^2}+A_{44}^s\frac{\partial^2\varphi_z}{\partial y^2}=0 \quad (23e)$$

Support types are typically used to rate FG plates. This study involves the exact solutions of the Eq. (23a)-(23e). In the present problem, where the FG plate is assumed to be simply supported at the plate boundaries, the succeeding settings are imposed

$$\begin{aligned} v_0 = w_0 = \theta = \theta_{,y} = \varphi = N_x = M_x^b = M_x^s = 0 \quad \text{at } x{=}0,a \\ u_0 = w_0 = \theta = \theta_{,x} = \varphi = N_y = M_y^b = M_y^s = 0 \quad \text{at } y{=}0,b \end{aligned} \quad (24)$$

Following the Navier process for resolving this problem, the following solutions are adapted for u_0, v_0, w_0, θ and ϕ_z, that satisfies the boundary conditions given as

$$\begin{Bmatrix} u_0 \\ v_0 \\ w_0 \\ \theta \\ \varphi_z \end{Bmatrix} = \begin{Bmatrix} U_{mn}\,cos(\alpha\,x)\,sin(\beta\,y) \\ V_{mn}\,sin(\alpha\,x)\,cos(\beta\,y) \\ W_{mn}\,sin(\alpha\,x)\,sin(\beta\,y) \\ X_{mn}\,sin(\alpha\,x)\,sin(\beta\,y) \\ \Phi_{mn}\,sin(\alpha\,x)\,sin(\beta\,y) \end{Bmatrix} \quad (25)$$

Where U_{mn}, V_{mn}, W_{mn},X_{mn} and Φ_{mn} are arbitrary parameters.

The transverse mechanical load q is assumed to be a double Fourier series shape and expressed as

$$\begin{aligned} q(x,y) &= \sum_{m=1,3,5}^{\infty}\sum_{n=1,3,5}^{\infty} q_{mn}\,sin(\alpha\,x)\,sin(\beta\,y) \\ q_{mn} &= \frac{4}{ab}\int_0^b\int_0^a q(x,y)\;sin(\alpha\,x)\,sin(\beta\,y)dxdy \end{aligned} \quad (26)$$

The values of q_{mn} using Eq. (26) are set as follows

$$\text{For SDL } \Rightarrow\; q_{mn} = q_0 \quad if\ (m=n=1) \quad (27a)$$

$$\text{For UDL} \Rightarrow\; q_{mn} = \begin{cases} \frac{16\,q_0}{m\,n\,\pi^2} & m,n = 1,3,5\ \ldots \\ 0 & m,n = 2,4,6\ \ldots \end{cases} \quad (27b)$$

$$\text{For CCL} \Rightarrow q_{mn} = \frac{4\,p_0}{a\,b}\,sin\left(\frac{m\,\pi\,x}{a}\right)\,sin\left(\frac{n\,\pi\,y}{b}\right) \quad \text{Avec } m=25\,, n=25\,, p_0 = q_0\,(a\,b) \quad (27c)$$

$$\text{For PDL} \Rightarrow\; q_{mn} = \begin{cases} \frac{16\,q_0}{m\,n\,\pi^2}X_mY_n & m,n = 1,3,5\ \ldots \\ 0 & m,n = 2,4,6\ \ldots \end{cases}$$
$$X_m = \left[sin\left(\frac{m\,\pi}{a}x_0\right)\right]\left[sin\left(\frac{m\,\pi}{2\,a}a_0\right)\right]$$
$$Y_n = \left[sin\left(\frac{n\,\pi}{b}y_0\right)\right]\left[sin\left(\frac{n\,\pi}{2\,b}b_0\right)\right] \quad (27d)$$

The substitution of Eq. (25) and Eq. (26) into Eqs. (23a)-(23e) shows that the analytical solutions of the present case may be established through

$$[a_{ij}]\{\delta\} = \{F\} \text{ with } i,j = 1,2,3,4\ \&\ 5. \quad (28)$$

Table 2 FG plate material characteristics

Properties	Mechanical case	
	Aluminum	Alumina
E	70	380
υ	0.3	0.3

In which

$$\{F\} = \begin{Bmatrix} F_1 = 0 \\ F_2 = 0 \\ F_3 = -qmn \\ F_4 = 0 \\ F_5 = 0 \end{Bmatrix} \text{ and } \{\delta\} = \begin{Bmatrix} U_{mn} \\ V_{mn} \\ W_{mn} \\ X_{mn} \\ \Phi_{mn} \end{Bmatrix} \tag{29}$$

And

$$\begin{aligned}
a_{11} &= -A_{11}\alpha^2 - A_{66}\beta^2 \\
a_{12} &= -(A_{66} + A_{12})\alpha\beta \\
a_{13} &= B_{11}\alpha^3 - (-B_{12} - 2B_{66})\alpha\beta^2 \\
a_{14} &= -BS_{66}(Ak_1 + Bk_2)\alpha\beta^2 + (BS_{11}k_1 + BS_{12}k_2)\alpha \\
a_{15} &= A_{13}\alpha \\
a_{22} &= -A_{22}\beta^2 - A_{66}\alpha^2 \\
a_{23} &= B_{22}\beta^3 + (B_{12} + 2B_{66})\alpha^2\beta \\
a_{24} &= -BS_{66}(Ak_1 + Bk_2)\alpha^2\beta + (BS_{12}k_1 + BS_{11}k_2)\beta \\
a_{25} &= A_{23}\beta \\
a_{33} &= -D_{11}\alpha^4 - 2(D_{12} + 2D_{66})\alpha^2\beta^2 - D_{22}\beta^4 - K_w - K_p(\alpha^2 + \beta^2) \\
a_{34} &= -(DS_{11}k_1 + DS_{12}k_2)\alpha^2 - (DS_{12}k_1 + DS_{22}k_2)\beta^2 + 2DS_{66}(Ak_1 + Bk_2)\alpha^2\beta^2 \\
a_{35} &= -B_{13}\alpha^2 - B_{23}\beta^2 \\
a_{44} &= -(k_1A)^2AS_{55}\alpha^2 - (k_2B)^2AS_{44}\beta^2 - HS_{66}(Ak_1 + Bk_2)^2\alpha^2\beta^2 \\
&\quad -k_1(HS_{11}k_1 + HS_{12}k_2) - k_2(HS_{12}k_1 + HS_{22}k_2) \\
a_{45} &= -Ak_1AS_{55}\alpha^2 - k_2BAS_{44}\beta^2 - BS_{13}k_1 - BS_{23}k_2 \\
a_{55} &= -AS_{55}\alpha^2 - AS_{44}\beta^2 - A_{33}
\end{aligned} \tag{30}$$

Where $[a_{ij}]$ is the stiffness matrix, $\{F\}$ is the force vector, and $\{\delta\}$ is the vector of unknowns.

3. Numerical results and discussion

This section is dedicated to the treatment of the outcomes obtained by analyzing the thermo-hygro-mechanical bending behavior of the FG plate while considering the presence of two elastic foundation parameters. This section is divided into three parts: the first is devoted to the validation of the results, the second presents a parametric study, and the last discusses the consequences of using different power laws on the behavior of FG plates on uniform and variable foundations. The FG plate is manufactured using a titanium alloy (Ti-6Al-4V) and zirconia (ZrO2). The mechanical characteristics of the plate, namely Young's modulus E, thermal expansion α, and moisture

Table 3 Nondimensionalized deflection $\bar{w}$ (0) of and the in-plane normal stress $\bar{\sigma}_{xx}$ $(h/3)$ in FG square plates under sinusoidal loads

k	Theory	$\bar{w}$			$\bar{\sigma}_{xx}$		
		a/h			*a/h*		
		4	10	100	4	10	100
1	Zenkour *et al.* (2014)	0.6896	0.5680	0.5446	0.5706	1.4159	14.1343
	Present Quasi-3D	0.6910	0.5691	0.5458	0.5805	1. 4486	14. 4784
4	Zenkour *et al.* (2014)	1.0970	0.8403	0.7910	0.4181	1.0802	10.8630
	Present Quasi-3D	1.0984	0.8420	0.7927	0.4307	1.1202	11.2813
10	Zenkour *et al.* (2014)	1.3333	0.9807	0.9130	0.3033	0.8031	8.1112
	Present Quasi-3D	1.3353	0.9816	0.9138	0.3146	0.8388	8.4844

concentration expansion β, are listed in Table 1. The Poisson's ratio is presumed to be constant $\upsilon = 0{,}3$.

The numerical results of this investigation are presented in terms of non-dimensional deflection and stresses. The calculation formulas for the dimensionless terms are as follows

$$\begin{gathered}\overline{w} = \frac{10^2 D}{q_0 a^4} w\left(\frac{a}{2},\frac{b}{2},\frac{z}{h}\right), w* = \frac{10h^3 E_c}{q_0 a^4} w\left(\frac{a}{2},\frac{b}{2},\frac{z}{h}\right),\\ w** = \frac{100h}{q_0 a^2} w\left(\frac{a}{2},\frac{b}{2},\frac{z}{h}\right), \sigma_1 = \frac{h}{q_0 a}\sigma_{xx}\left(\frac{a}{2},\frac{b}{2},\frac{z}{h}\right),\\ \sigma_3 = \frac{h}{q_0 a}\sigma_{zz}\left(\frac{a}{2},\frac{b}{2},\frac{z}{h}\right), \sigma_4 = \frac{10}{q_0}\sigma_{yx}\left(\frac{a}{2},0,\frac{z}{h}\right),\\ \sigma_5 = \frac{10h}{q_0 a}\sigma_{xz}\left(0,\frac{b}{2},\frac{z}{h}\right), \sigma_6 = \frac{h}{q_0 a}\sigma_{xy}\left(0,0,\frac{z}{h}\right),\\ k_w = \frac{a^4}{D}K_w, \mathrm{k}_p = \frac{a^2}{D}K_p, D = \frac{h^3 Ec}{12(1-\nu^2)}\end{gathered} \tag{31}$$

3.1 Comparative study

Table 2 provides a comparative analysis of the non-dimensionalized deflection ($\bar{w}$) and in-plane normal stress ($\bar{\sigma}_{xx}$) for functionally graded square plates subjected to sinusoidal loading. The results obtained from the current theoretical framework demonstrate a strong agreement with those of Zenkour *et al.* (2014) for the Quasi-3D theory ($\varepsilon_z \neq 0$). Notably, the deflection ($\bar{w}$) exhibits a decreasing trend with increasing side-to-thickness ratio (*a/h*) and decreasing volume fraction index (*k*), whereas the in-plane normal stress ($\bar{\sigma}_{xx}$) increases.

Table 4 presents a comparative analysis of the non-dimensional stresses and deflection for isotropic homogeneous and functionally graded square plates with varying volume fraction indices. The results are compared with those of Zenkour *et al.* (2014) based on the transverse shear and normal deformation plate theory. It was observed that the shear stress, axial stress, and deflection decreased with increasing foundation parameters (*kw*, *kp*). The volume fraction index (*k*) significantly influences the stress and deflection behaviors of both isotropic homogeneous and functionally graded plates. The deflection increases with increasing volume fraction index (*k*) owing to the reduction in bending stiffness, which is maximum for a fully ceramic plate (*k*=0). In the absence of elastic foundations, the stresses in the fully ceramic and fully metallic plates are identical, demonstrating that the stresses are independent of the modulus of elasticity for

Table 4 Nondimensionalized deflection $\bar{w}(0)$ of and stresses σi in FG square plates resting on elastic foundations under sinusoidal loads (a=10 h)

$(\boldsymbol{w}^*, \boldsymbol{\sigma_i})$	k_w	k_p	Theory	k					
				0	1	2	5	10	∞
$\boldsymbol{w}^*$	0	0	Himeur *et al.* (2022) 2D	0.29605	0.58895	0.75732	0.91155	1.00880	1.60715
			Himeur *et al.* (2022) 3D	0.29415	0.56939	0.72195	0.87418	0.98200	1.59679
			Zenkour *et al.* (2014)	0.29334	0.56802	0.71988	0.87256	0.98072	1.59239
			Present [3D]	0.29333	0.56802	0.71987	0.87256	0.98074	1.59239
	100	10	Himeur *et al.* (2022) 2D	0.16390	0.22618	0.24729	0.26175	0.26921	0.29890
			Himeur *et al.* (2022) 3D	0.16403	0.22440	0.24467	0.26004	0.26895	0.30093
			Zenkour *et al.* (2014)	0.16379	0.22419	0.24445	0.25994	0.26893	0.30081
			Present [3D]	0.16379	0.22420	0.24445	0.25994	0.26893	0.30080
$\boldsymbol{\sigma_1}$ (h/2)	0	0	Himeur *et al.* (2022) 2D	1.99472	3.08569	3.60760	4.24608	5.08624	1.99472
			Himeur *et al.* (2022) 3D	2.03137	3.11958	3.64669	4.27100	5.10271	2.03137
			Zenkour *et al.* (2014)	2.12463	3.27707	3.82256	4.47146	5.3291	2.12463
			Present [3D]	1.85797	3.27709	3.82256	4.47143	5.32909	2.12463
	100	10	Himeur *et al.* (2022) 2D	1.10434	1.18501	1.17800	1.21927	1.35730	0.37098
			Himeur *et al.* (2022) 3D	1.13279	1.22941	1.23585	1.27047	1.39753	0.38283
			Zenkour *et al.* (2014)	1.18631	1.29346	1.29805	1.33209	1.46131	0.40135
			Present [3D]	1.18632	1.29346	1.29805	1.33208	1.46132	0.40134
$\boldsymbol{\sigma_6}$ (-h/3)	0	0	Himeur *et al.* (2022) 2D	0.70662	0.61108	0.54418	0.57561	0.58953	0.70662
			Himeur *et al.* (2022) 3D	0.70068	0.56582	0.49413	0.52449	0.54795	0.70068
			Zenkour *et al.* (2014)	0.69856	0.56467	0.49269	0.52346	0.54777	0.69856
			Present [3D]	0.69810	0.56468	0.49268	0.52346	0.54778	0.69856
	100	10	Himeur *et al.* (2022) 2D	0.39121	0.23468	0.17769	0.16529	0.15732	0.13142
			Himeur *et al.* (2022) 3D	0.39073	0.22299	0.16746	0.15602	0.15007	0.13205
			Zenkour *et al.* (2014)	0.39005	0.22288	0.16731	0.15594	0.15021	0.13196
			Present [3D]	0.39006	0.22287	0.16731	0.15594	0.15021	0.13196
$\boldsymbol{0.1\,\sigma_5}$ (0)	**0**	**0**	Himeur *et al.* (2022) 2D	0.24193	0.24193	0.22200	0.19660	0.21491	0.24193
			Himeur *et al.* (2022) 3D	0.24168	0.24168	0.22178	0.19642	0.21472	0.24168
			Zenkour *et al.* (2014)	0.24541	0.24541	0.22581	0.20107	0.21916	0.24541
			Present [3D]	0.22935	0.24540	0.22581	0.20107	0.21915	0.24541
	100	10	Himeur *et al.* (2022) 2D	0.13394	0.09291	0.07249	0.05646	0.05735	0.04499
			Himeur *et al.* (2022) 3D	0.13477	0.09524	0.07516	0.05843	0.05881	0.04555
			Zenkour *et al.* (2014)	0.13703	0.09686	0.07668	0.0599	0.06009	0.04636
			Present [3D]	0.13703	0.09686	0.07667	0.05990	0.06009	0.04635

homogeneous materials. The excellent agreement between the present results and those reported in Table 4 validates the effectiveness of the proposed method.

3.2 Parametric study

3.2.1 Numerical results

This study investigated the bending behavior of functionally graded plates under sinusoidal and

Table 5 The deflection$\bar{w}$of a square nanoplate without or resting on elastic foundations for different values of inhomogeneity parameter *a/h*=10

k_w	k_p	μ	k					
			0	1	2	3	5	10
0	0	0	2.93335	5.68020	7.19880	7.95496	8.72560	9.80723
		1	3.51237	6.80143	8.61977	9.52519	10.4480	11.7431
		2	4.09138	7.92262	10.0407	11.0954	12.1703	13.6790
		3	4.67043	9.04385	11.4617	12.6657	13.8927	15.6148
		4	5.24943	10.1651	12.8827	14.2359	15.6151	17.5507
100	0	0	2.31709	3.74764	4.35241	4.61768	4.86791	5.18905
		1	2.66399	4.20500	4.83428	5.10633	5.36096	5.68488
		2	2.98433	4.60818	5.25103	5.52554	5.78075	6.10303
		3	3.28103	4.96633	5.61507	5.88913	6.14247	6.46030
		4	3.55663	5.28652	5.93583	6.20749	6.45738	6.76924
100	10	0	1.63788	2.24197	2.44452	2.52595	2.59943	2.68928
		1	1.80392	2.39800	2.58948	2.66548	2.73368	2.81661
		2	1.94532	2.52394	2.70446	2.77539	2.83880	2.91557
		3	2.06716	2.62773	2.79789	2.86421	2.92334	2.99471
		4	2.17327	2.71473	2.87531	2.93748	2.99280	3.05943

Table 6 Dimensionless deflection $\overline{w}$ and normal stress $\overline{\sigma}_{xx}$ and transverse shear stress $\overline{\sigma}_{xz}$ of FGM square plates under uniform loads without Kerr foundations (Kl=100)

(*Ku*, *Ks*)	k	$\overline{w}\left(\frac{a}{2},\frac{b}{2},0\right)$			$\overline{\sigma}_{xx}\left(\frac{a}{2},\frac{b}{2},\frac{h}{2}\right)$			$\overline{\sigma}_{xz}\left(0,\frac{b}{2},0\right)$		
		a/h								
		5	10	20	5	10	20	5	10	20
(0, 0)	0	0.52445	0.46380	0.44853	1.51452	2.94041	5.83643	0.48433	0.49871	0.50591
	1	1.00068	0.89823	0.87244	2.33160	4.51347	8.95208	0.48433	0.49872	0.50591
	2	1.28306	1.13847	1.10208	2.73395	5.27327	10.44889	0.44382	0.45737	0.46414
	5	1.61690	1.37660	1.31614	3.22499	6.16787	12.19510	0.39209	0.40463	0.41091
	10	1.84243	1.54561	1.47092	3.84726	7.37103	14.58042	0.42856	0.44232	0.44919
	∞	2.84700	2.51779	2.43487	1.51451	2.94040	5.83639	0.48433	0.49871	0.50591
(100, 0)	0	0.51998	0.46358	0.44852	1.50049	2.93891	5.83624	0.48108	0.49854	0.50590
	1	0.98450	0.89741	0.87240	2.29054	4.50902	8.95151	0.47816	0.49836	0.50591
	2	1.25649	1.13715	1.10200	2.67216	5.26657	10.44826	0.43656	0.45696	0.46413
	5	1.57460	1.37466	1.31603	3.13298	6.15841	12.19398	0.38399	0.40420	0.41088
	10	1.78765	1.54316	1.47078	3.72288	7.35832	14.57884	0.41852	0.44177	0.44915
	∞	2.71990	2.51130	2.43450	1.44105	2.93217	5.83548	0.46729	0.49773	0.50585
(10, 100)	0	0.29583	0.39621	0.43857	0.82243	2.48480	5.58960	0.30001	0.44006	0.49013
	1	0.40252	0.67470	0.80757	0.87761	3.32083	8.24213	0.22772	0.39816	0.47628
	2	0.43969	0.80120	1.00049	0.86760	3.61694	9.42223	0.18232	0.34711	0.43041
	5	0.47076	0.91131	1.17370	0.86701	3.96335	10.7886	0.13824	0.29247	0.37576
	10	0.48782	0.98213	1.29521	0.94033	4.53426	12.7256	0.13826	0.30958	0.40674
	∞	0.53990	1.30127	1.98828	0.25688	1.44442	4.69728	0.11948	0.29970	0.43250
(100, 100)	0	0.09839	0.23818	0.36538	0.25397	1.43440	4.68509	0.11837	0.29828	0.43170
	1	0.10711	0.31517	0.60420	0.21406	1.45112	6.03071	0.07350	0.22636	0.38215
	2	0.10916	0.33927	0.70564	0.19866	1.41920	6.46581	0.05443	0.18421	0.33082
	5	0.11072	0.35650	0.78709	0.19139	1.43041	7.00881	0.03779	0.14558	0.27838
	10	0.11171	0.36640	0.83961	0.20370	1.55701	7.96765	0.03624	0.14847	0.29412
	∞	0.11455	0.40178	1.08235	0.05131	0.40157	2.42609	0.02899	0.12829	0.27804

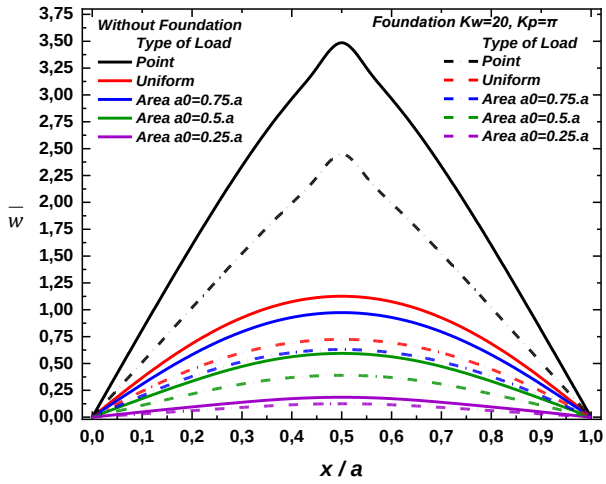

Fig. 2 Dimensionless deflections of FG plate under point load, uniform and partially distributed load (3/4, 1/2 and 1/4), where k=2, a/h=10, Kw=20, Kp=π

uniform loads. It analyzes the influence of various parameters, including the foundation type, power-law index, plate geometry, and stress and displacement distribution through the thickness under various partial loads.

Tables 5 and 6 present a parametric analysis of the non-dimensional stresses and deflections for isotropic homogeneous and functionally graded square nanoplates, considering varying scale parameters and side-to-thickness ratios (a/h). The dimensionless deflection increase with the increase of material index and the scale parameter's. The shear stress, axial stress, and deflection decreased with increasing Winkler-Pasternak (kw, kp) and Kerr (Ku, Ks) foundation parameters. The volume fraction index (k) significantly influenced the stress and deflection behaviors of both the isotropic homogeneous and functionally graded plates. The deflection increased with increasing side-to-thickness ratios (a/h) owing to a combination of reduced stiffness, increased shear deformation, and stress concentration, which was most pronounced in thin plates (a/h=20). In the absence of elastic foundations, the stresses in the fully ceramic and fully metallic plates were identical, indicating that for homogeneous materials, the stresses are independent of the modulus of elasticity.

3.2.2 Graphical illustration

Fig. 2 shows the dimensionless central deflection along the x-direction of the plate for different loads, distributed uniformly over (100%, 75%, and 25%) of the plate surface and point load, without a foundation and with a Winkler-Pasternak foundation model. It is evident that the highest values of the dimensionless central deflection are obtained for the concentrated load. However, the lowest values were obtained for loads uniformly distributed over 25% of the plate surface.

Fig. 3 shows the dimensionless central deflection along the x-direction of the plate for different loads, distributed uniformly over (100%, 75%, 25%) of the plate surface and point load, without foundation and with Kerr foundation model. It is evident that the highest values of the dimensionless central deflection are obtained for the concentrated load. However, the lowest values were obtained for loads uniformly distributed over 25% of the plate surface.

Fig. 4 shows the variation of the non-dimensional central deflection with respect to the

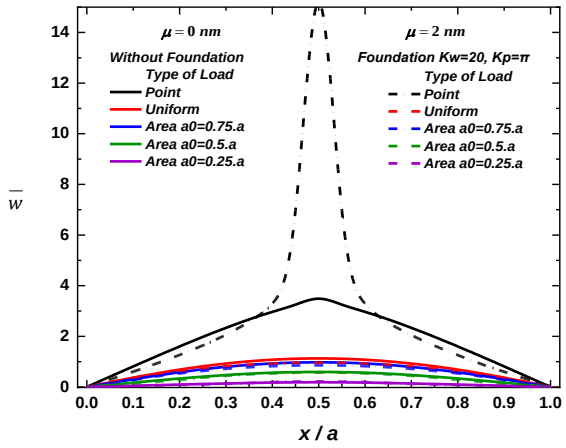

Fig. 3 Dimensionless deflections of FG nanoplate under point load, uniform and partially load (3/4, 1/2 and 1/4), where k=2, a/h=10, Kw=20, Kp=π

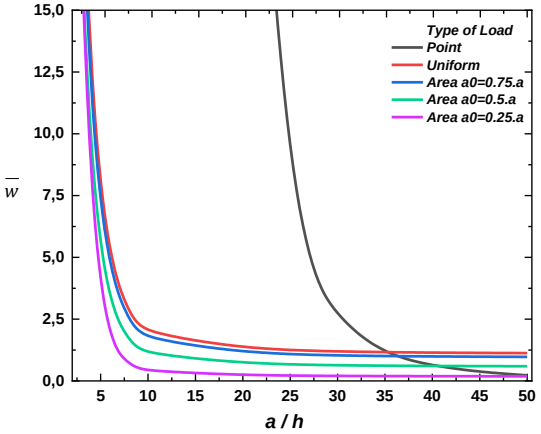

Fig. 4 The non-dimensional central deflections of square FG nanoplate as a function of side-to-thickness ratio, under *p*oint load, uniform and partially distributed load (3/4, 1/2 and 1/4), k=2

thickness ratio "a/h" subjected to mechanical loads (concentrated load and uniform distributed load 100%, 75%, and 50% of the surface of the plate without foundation). It can be observed that the non-dimensional central deflection decreases when the thickness ratio increases.

Fig. 5 presents the effect of the power-law index "k" on the dimensionless central deflection using various mechanical loads. Full ceramic plates exhibited the minimum non-dimensional central deflection. However, increasing the power-law index "k" leads to an increase in the non-dimensional central deflection.

Fig. 6 shows the effect of the geometrical ratio "b/a" on the dimensionless central deflection of the plate. It can be observed that the dimensionless central deflection increases as "b/a" increases. Regardless of the loading type, the deflection followed the same trend as the previous curves.

Figs. 7-8 shows the evolution of the dimensionless axial stress subjected to a uniformly distributed load over (100%, 75%, and 25%) of the plate surface and a central concentrated load,

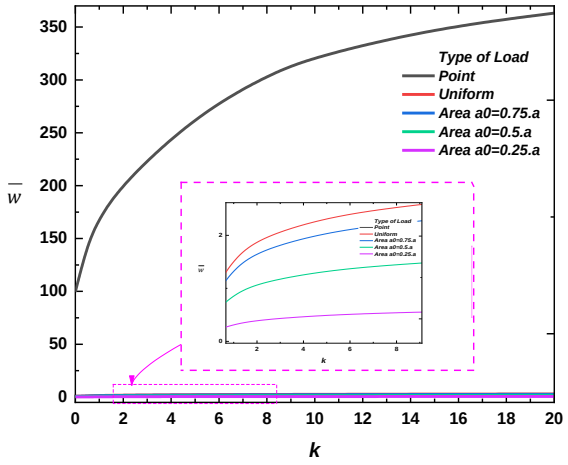

Fig. 5 Non-dimensional central deflections of FG nanoplate as a function of side-to-thickness ratio, under *p*oint load, uniform and partially distributed load (3/4, 1/2 and 1/4, k=2)

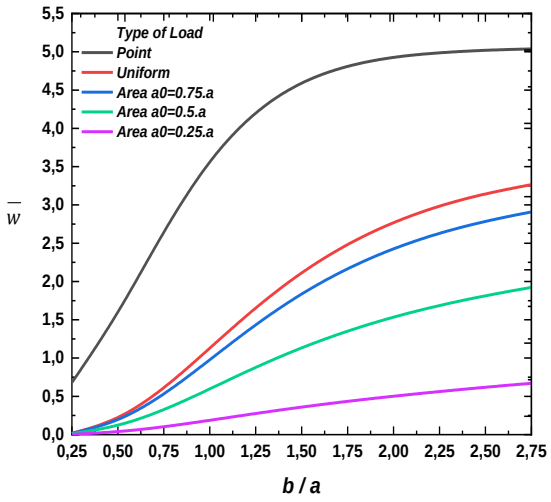

Fig. 6 The deflections of square PFGM plate as a function of aspect ratio "b/a", under point load, uniform and partially distributed load (3/4, 1/2 and 1/4), k=2 and a/h=10

without a foundation and with the Winkler-Pasternak model. As shown in Fig. 5, the effect of Winkler-Pasternak foundations and without foundation on the dimensionless normal stresses is significant. However, for the central concentrated load, the normal stresses were tensile at the top surface and compressive at the bottom surface for both loads.

Fig. 9 shows the dimensionless central deflection along the x-direction of the plate for a uniformly distributed load and variable-sized Kerr foundation. Moreover, the highest values of the dimensionless central deflection were obtained for the widest foundations. Fig. 10 shows the variation in the non-dimensionless transverse shear stresses for a uniformly distributed load on (100%, 75%, and 25%) of the plate surface and a point load. For these types of loading, the maximum dimensionless transverse shear stress depends on the loading type. In addition, the

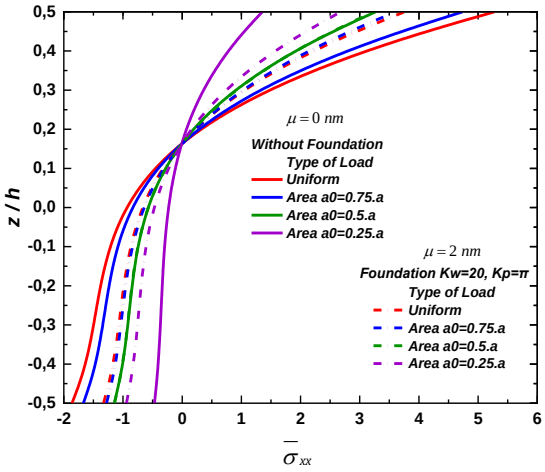

Fig. 7 The non-dimensional axial stresses $\overline{\sigma}_{xx}$ of square FG nanoplate as a function of z-direction under uniform load and partially load (3/4, 1/2 and 1/4) (k=2 and a/h=10)

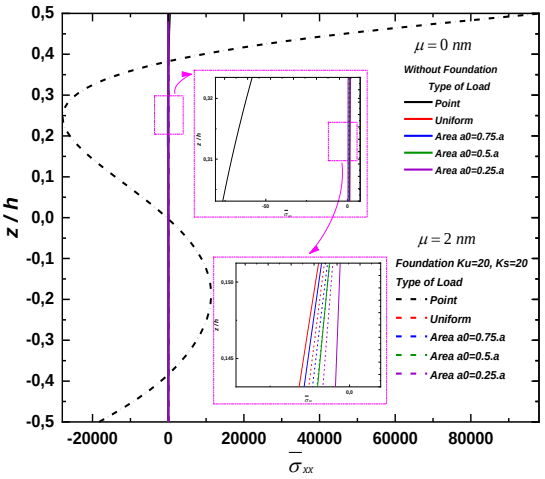

Fig. 8 The non-dimensional axial stresses $\overline{\sigma}_{xx}$ of square FG nanoplate as a function of z-direction under partially load (1/4, 1/2, 3/4 and1) and point load (k=2 and a/h=10)

evolution of the non-dimensionless transverse shear stresses was smooth for this type of loading. However, the magnitude of the shear stress was significantly higher for the point load case without any foundation. In contrast, when an elastic support is present, the shear stress values for the point load become closer to those observed under uniform distribution loading.

Fig. 11 shows the dimensionless axial stress through the plate thickness for a uniformly distributed load and a variable-sized Kerr foundation "*de*", Moreover, the highest values of the dimensionless normal stress were obtained for the widest foundation.

Fig. 12 shows the dimensionless transverse shear stress for a uniformly distributed load and variable-sized Kerr foundation "*de*", However, the highest values of the dimensionless transverse shear stress were obtained for the widest foundations.

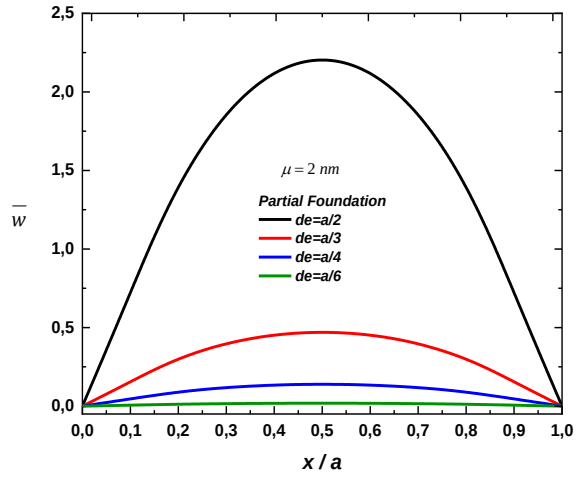

Fig. 9 Dimensionless central deflection of FG nanoplate under uniform load with a variable-sized Kerr foundation "*de*"(*k*=2, *a/h*=10, *Kl*=20, *Ku*=20, *Ks*=20)

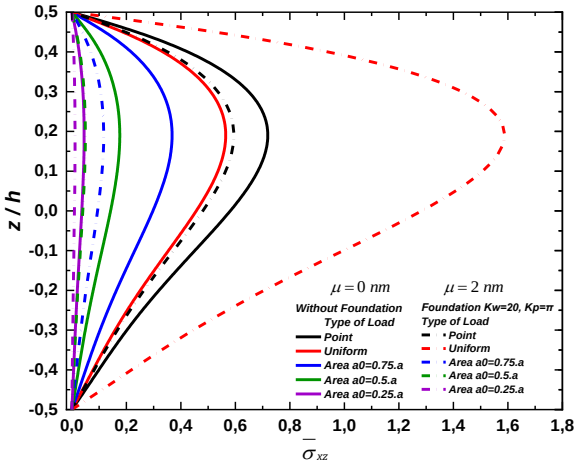

Fig. 10 The shear stresses $\overline{\sigma}_{xz}$ of an P-FGM the square nanoplate under uniform load, line load, point load and partially load (3/4 ,1/2 and 1/4), where *k*=2, *a/h*=10, *Kw*=20, *Kp*=π

Fig. 13 shows the dimensionless transverse displacement of FG nanoplate under partial distributed load "50%" resting on Kerr foundation model. The highest values of the dimensionless transverse displacement are obtained for the widest partial load.

4. Conclusions

In the present plate theory, the current analytical model is developed to investigate the bending behavior of simply supported FG plates exposed to several mechanical loads and resting on various elastic foundations (Winkler-Pasternak and Kerr). Moreover, virtual displacement is

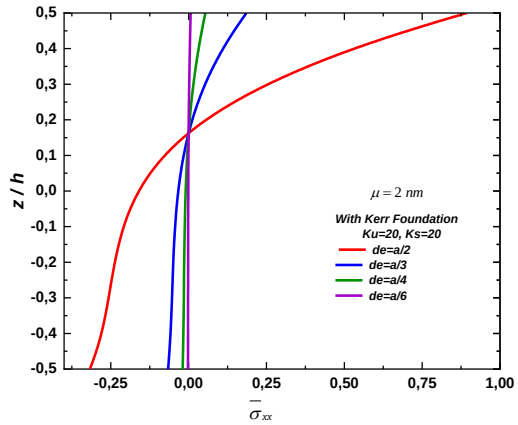

Fig. 11 The nondimensional axial stresses $\overline{\sigma}_{xx}$ of square P-FGM plate under partial loading "75%" and with a variable-sized Kerr foundation "*de*" (*k*=2, *a/h*=10, *Kl*=20, *Ku*=20, *Ks*=20)

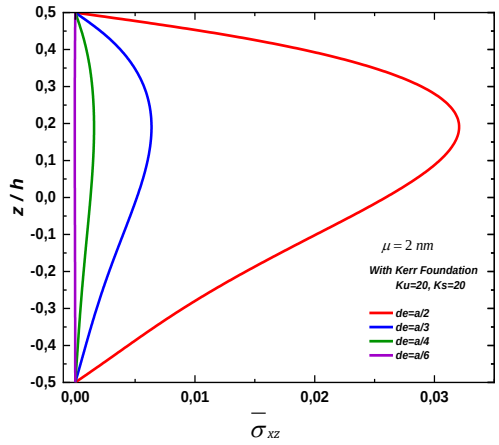

Fig. 12 The nondimensional shear stresses $\overline{\sigma}_{xz}$ of square FG nanoplate under partial loading "75%" and with a variable-sized Kerr foundation "*de*" (*k*=2, *a/h*=10, *Kl*=20, *Ku*=20, *Ks*=20)

applied to obtain the principal equations of the equilibrium. These equations were solved numerically using Navier's technique. The results are then presented by including and excluding the effects of the transverse normal strain. The non-dimensional deflection, normal stress, and shear stress values with the effect of scale parameter, side-to-thickness ratio *a/h*, power law index *k*, load type, and Winkler-Pasternak *(Kw*, *Kp)* and Kerr *(Ku*, *Ks)* foundation parameters are compared and validated with known results in the literature.

References

Abdelrahman, A.A., Ashry, M., Alshorbagy, A.E., Eltaher, M.A. and Abdalla, W.S. (2024), "On the dynamic behavior of functionally graded cracked beams resting on winkler foundation under moving load", *Steel Compos. Struct.*, **53**(2), 169-194. https://doi.org/10.12989/scs.2024.53.2.169.

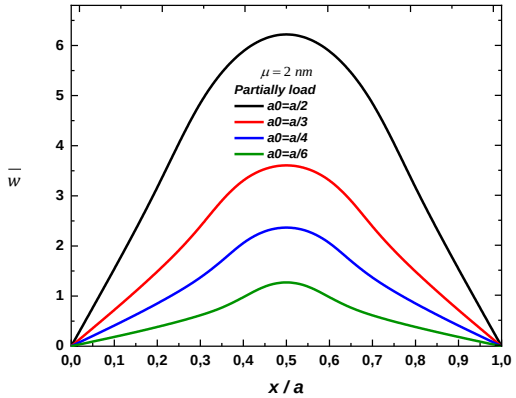

Fig. 13 The dimensionless central deflection of square FG Nanoplate under partial loading "50%" resting on Kerr foundation (k=2, a/h=10, Kl=20, $K\mu$=20, Ks=20 and $\mu = 2$ nm)

Adiyaman, G. and Turan, M. (2025), "Bending and buckling analysis of porous 2D functionally graded beams with exponential material property variation", *Iran. J. Sci. Technol. Trans. Civil Eng.*, **49**, 1359-1386. https://doi.org/10.1007/s40996-024-01508-4.

Ameur, M., Tounsi, A., Mechab, I. and El Bedia, A.A. (2011), "A new trigonometric shear deformation theory for bending analysis of functionally graded plates resting on elastic foundations", *KSCE J. Civil Eng.*, **15**, 1405-1414. https://doi.org/10.1007/s12205-011-1361-z.

Chen, W.R., Chiu, L.H. and Lin, C.H. (2024), "Vibration of elastically supported bidirectional functionally graded sandwich Timoshenko beams on an elastic foundation", *Struct. Eng. Mech.*, **91**(2), 197-209. https://doi.org/10.12989/sem.2024.91.2.197.

Chitour, M., Bouhadra, A., Benguediab, M., Mansouri, K., Menasria, A. and Tounsi, A. (2022), "A new high order theory for buckling temperature analysis of functionally graded sandwich plates resting on elastic foundations", *Nano-Electron. Phys.*, **14**(3), 03028. https://doi.org/10.21272/jnep.14(3).03028.

Chitour, M., Bouhadra, A., Benguediab, S., Saoudi, A., Menasria, A. and Tounsi, A. (2022), "Effect of phase contrast and geometrical parameters on bending behavior of sandwich beams with FG isotropic face sheets", *J. Nano-Electron. Phys.*, **14**(5), 05016. https://doi.org/10.21272/jnep.14(5).05016.

Do, N.T. and Pham, Q.H. (2024), "Nonlinear static analysis of functionally graded porous sandwich plates resting on Kerr foundation", *Mech. Adv. Mater. Struct.*, **31**(22), 5678-5691. https://doi.org/10.1080/15376494.2023.2218845.

Eghbali, M. and Hosseini, S.A. (2024), "An accurate analytical exploration for dynamic response of thermo-electric CNTRC beams under driving harmonic and constant loads resting on Pasternak foundation", *Adv. Nano Res.*, **16**(6), 549-564. https://doi.org/10.12989/anr.2024.16.6.549.

Faicel, K., Abderahmane, M., Belgacem, M., Abdelhakim, B., Fouad, B., Soumia, B., ... & Abdelouahed, T. (2022), "Thickness stretching and nonlinear hygro-thermo-mechanical loading effects on bending behavior of FG beams", *Struct. Eng. Mech.*, **84**(6), 783-798. https://doi.org/10.12989/sem.2022.84.6.783.

Fan, Y.H. and She, G.L. (2025), "Nonlinear transient response of graphene platelets reinforced metal foams beam considering initial geometrical imperfection and viscoelastic elastic foundation", *Comput. Concrete*, **35**(1), 59-70. https://doi.org/10.12989/cac.2025.35.1.059.

Foroutan, K. and Dai, L. (2024), "Nonlinear free and forced vibrations of oblique stiffened porous FG shallow shells embedded in a nonlinear elastic foundation", *Struct. Eng. Mech.*, **89**(1), 33-46. https://doi.org/10.12989/sem.2024.89.1.033.

Han, J.B. and Liew, K. (1997), "Numerical differential quadrature method for Reissner/Mindlin plates on two-parameter foundations", *Int. J. Mech. Sci.*, **39**(9), 977-989. https://doi.org/10.1016/S0020-7403(97)00001-5.

He, Y.J. and She, G.L. (2024), "Nonlinear forced vibration of imperfect FG beams with hygro-thermal factor", *Struct. Eng. Mech.*, **92**(2), 163-172. https://doi.org/10.12989/sem.2024.92.2.163.

Himeur, N., Mamen, B., Benguediab, S., Bouhadra, A., Menasria, A., Bouchouicha, B., ... & Benguediab, M. (2022), "Coupled effect of variable Winkler-Pasternak foundations on bending behavior of FG plates exposed to several types of loading", *Steel Compos. Struct.*, **44**(3), 353-369. https://doi.org/10.12989/scs.2022.44.3.353.

Hoang, V.N.V. and Thanh, P.T. (2023), "Influences of arbitrary-distributed Kerr foundation on free vibration and nonlinear transient response of functionally graded plate in thermal environment", *Thin Wall. Struct.*, **188**, 110802. https://doi.org/10.1016/j.tws.2023.110802.

Hoang, V.N.V., Shi, P., Toledo, L. and Vu, H. (2024), "Thermal vibration analysis of FG-GPLRC doubly curved shells partially resting on Kerr foundation based on higher-order shear deformation theory", *Thin Wall. Struct.*, **195**, 111357. https://doi.org/10.1016/j.tws.2023.111357.

Houari, M.S.A., Bessaim, A., Bezzina, S., Tounsi, A., Daikh, A.A., Garg, A. and Belarbi, M.O. (2024), "Thermoelastic bending analysis of thick functionally graded sandwich plates with arbitrary graded material properties using a novel quasi-3D HSDT", *Arch. Civil Mech. Eng.*, **24**(2), 80. https://doi.org/10.1007/s43452-024-00898-6.

Huang, Z., Han, M., Wang, X. and Chu, F. (2023). Bending analysis of two different types of functionally graded material porous sandwich plates", *Arch. Appl. Mech.*, **93**(8), 3071-3091. https://doi.org/10.1007/s00419-023-02425-0.

Kahya, V. and Turan, M. (2018), "Vibration and buckling of laminated beams by a multi-layer finite element model", *Steel Compos. Struct.*, **28**(4), 415-426. https://doi.org/10.12989/scs.2018.28.4.415.

Kahya, V.O.L.K.A.N. and Turan, M.E.H.M.E.T. (2017), "Bending of laminated composite beams by a multi-layer finite element based on a higher-order theory", *Acta Physica Polonica A*, **132**(3), 473-475. https://doi.org/10.12693/APhysPolA.132.473.

Kumar, R., Lal, A., Sutaria, B., Dehury, R.K., Joshi, Y.G. and Gupta, V.S. (2024), "Bending analysis of a porous functionally graded sandwich plate with a hole resting on an elastic foundation", *Acta Mechanica*, **235**(8), 5061-5078. https://doi.org/10.1007/s00707-024-03989-w.

Li, S.R., Zhang, F. and Liu, R.G. (2024), "Classical and homogenized expressions for the bending solutions of FGM plates based on the four variable plate theories", *Mech. Adv. Mater. Struct.*, **31**(15), 3413-3424. https://doi.org/10.1080/15376494.2023.2177909.

Mekerbi, M., Benyoucef, S., Mahmoudi, A., Tounsi, A., Bousahla, A.A. and Mahmoud, S. (2021), "Thermodynamic behavior of functionally graded sandwich plates resting on different elastic foundation and with various boundary conditions", *J. Sandw. Struct. Mater.*, **23**(3), 1028-1057. https://doi.org/10.1177/1099636219851281.

Meski, K., Boutrid, A., Menasria, A., Bouhadra, A., Mamen, B., Tounsi, A. and Cuong-Le, T. (2024), "Analytical modeling of flexural behavior of advanced composite sandwich beams under nonlinear hygro-thermo-mechanical loads", *Multiscale Multidisc. Model. Exper. Des.*, **7**(5), 4701-4719. https://doi.org/10.1007/s41939-024-00414-6.

Mohammed, A.J., Mohammed, B.A., Kadhom, H.K., Taki, A.G. and Tahouneh, V. (2024), "A semi-analytical study for vibration analysis of damaged core laminated cylindrical shell with functionally graded CNTs reinforced face sheets resting on a two-parameter elastic foundation", *Adv. Nano Res.*, **17**(4), 301-313. https://doi.org/10.12989/ANR.2024.17.4.301.

Najafi, M., Ahmadi, I. and Sladek, V. (2024), "A new three-dimensional model for free vibration analysis of functionally graded nanoplates resting on an elastic foundation", *Steel Compos. Struct.*, **52**(3), 273-291. https://doi.org/10.12989/scs.2024.52.3.273.

Nebab, M., Ait Atmane, H., Bennai, R. and Tounsi, A. (2019), "Effect of variable elastic foundations on static behavior of functionally graded plates using sinusoidal shear deformation", *Arab. J. Geosci.*, **12**(24), 809. https://doi.org/10.1007/s12517-019-4871-5.

Park, M. and Choi, D.H. (2018), "A simplified first-order shear deformation theory for bending, buckling and free vibration analyses of isotropic plates on elastic foundations", *KSCE J. Civil Eng.*, **22**, 1235-1249. https://doi.org/10.1007/s12205-017-1517-6.

Rachid, A., Ouinas, D., Lousdad, A., Zaoui, F.Z., Achour, B., Gasmi, H., ... & Tounsi, A. (2022), "Mechanical behavior and free vibration analysis of FG doubly curved shells on elastic foundation via a new modified displacements field model of 2D and quasi-3D HSDTs", *Thin Wall. Struct*., **172**, 108783. https://doi.org/10.1016/j.tws.2021.108783.

Salehipour, H., Shahmohammadi, M.A. and Civalek, Ö. (2024), "Natural frequencies and modal shapes of folded sandwich plates made of porous core and FG-CNTRC coating layers resting on two parameters elastic foundation", *Aerosp. Sci. Technol*., **148**, 109077. https://doi.org/10.1016/j.ast.2024.109077.

She, G.L., Li, Y.P., He, Y. and Song, J.P. (2024), "Thermal post-buckling analysis of graphene platelets reinforced metal foams beams with initial geometric imperfection", *Comput. Concrete*, **33**(3), 241-250. https://doi.org/10.12989/cac.2024.33.3.241.

Shen, X., Li, T., Xu, L., Kiarasi, F., Babaei, M. and Asemi, K. (2024), "Free vibration analysis of FG porous spherical cap reinforced by graphene platelet resting on Winkler foundation", *Adv. Nano Res.*, **16**(1), 11-26. https://doi.org/10.12989/anr.2024.16.1.011.

Slimani, R., Menasria, A., Ali Rachedi, M., Mourad, C., Refrafi, S., Nimer, A.A., ... & Mamen, B. (2024), "A novel quasi-3D refined HSDT for static bending analysis of porous functionally graded plates", *J. Comput. Appl. Mech*., **55**(3), 519-537. https://doi.org/10.22059/jcamech.2024.372417.968.

Soltani, M., Momenian, M. and Civalek, O. (2024), "Stability analysis of sandwich double nanobeam-system with varying cross-section interconnected by Kerr-type three-parameter elastic layer", *Thin Wall. Struct.*, **204**, 112249. https://doi.org/10.1016/j.tws.2024.112249.

Tamrabet, A., Mamen, B., Menasria, A., Bouhadra, A., Tounsi, A., Ghazwani, M.H., ... & Mahmoud, S.R. (2023), "Buckling behaviors of FG porous sandwich plates with metallic foam cores resting on elastic foundation", *Struct. Eng. Mech.*, **85**(3), 289-304. https://doi.org/10.12989/sem.2023.85.3.289.

Thai, H.T., Park, M. and Choi, D.H. (2013), "A simple refined theory for bending, buckling, and vibration of thick plates resting on elastic foundation", *Int. J. Mech. Sci.*, **73**, 40-52. https://doi.org/10.1016/j.ijmecsci.2013.03.017.

Turan, M. (2022), "Bending analysis of two-directional functionally graded beams using trigonometric series functions", *Arch. Appl. Mech*., **92**, 1841-1858. https://doi.org/10.1007/s00419-022-02152-y.

Turan, M. (2024), "Mixed series solution for vibration and stability of porous bi-directional functionally graded beams", *Arch. Appl. Mech*., **94**, 1785-1806. https://doi.org/10.1007/s00419-024-02611-8.

Turan, M. and Adiyaman, G. (2024), "Free vibration and buckling analysis of porous two-directional functionally graded beams using a higher-order finite element model", *J. Vib. Eng. Technol*., **12**, 1133-1152. https://doi.org/10.1007/s42417-023-00898-5.

Turan, M. and Adiyaman, G.A. (2023), "New higher-order finite element for static analysis of two-directional functionally graded porous beams", *Arab. J. Sci. Eng*., **48**, 13303-13321. https://doi.org/10.1007/s13369-023-07742-8.

Turan, M. and Kahya, V. (2021), "Free vibration and buckling analysis of functionally graded sandwich beams by Navier method", *Gazi Univ. J. Eng. Arch. Facult.*, **36**(2), 743-758. https://doi.org/10.17341/gazimmfd.599928.

Turan, M., Kahya, V., Yaylacı, E. and Yaylaci, M. (2025), "A shear deformable numerical approaches for the static analysis of bi-directional functionally graded beams", *Adv. Nano Res.*, **18**(2). https://doi.org/10.12989/anr.2025.18.2.143.

Turan, M., Uzun Yaylacı, E. and Yaylacı, M. (2023), "Free vibration and buckling of functionally graded porous beams using analytical, finite element, and artificial neural network methods", *Arch. Appl. Mech*., **93**, 1351-1372. https://doi.org/10.1007/s00419-022-02332-w.

Wu, C.P., Chiu, K.H. and Wang, Y.M. (2011), "RMVT-based meshless collocation and element-free Galerkin methods for the quasi-3D analysis of multilayered composite and FGM plates", *Compos. Struct.*, **93**(2), 923-943. https://doi.org/10.1016/j.compstruct.2010.07.001.

Yaghoobi, H. and Fereidoon, A. (2014), "Mechanical and thermal buckling analysis of functionally graded plates resting on elastic foundations: An assessment of a simple refined nth-order shear deformation theory", *Compos. Part B: Eng.*, **62**, 54-64. https://doi.org/10.1016/j.compositesb.2014.02.014.

Yushan, X. and Zhen, W. (2024), "Non-linear bending analysis and control of graphene-platelets-reinforced

porous sandwich plates with piezoelectric layer subjected to electromechanical loading", *Appl. Math. Model.*, **137**, 115708. https://doi.org/10.1016/j.apm.2024.115708.

Zaoui, F.Z., Ouinas, D. and Tounsi, A. (2019), "New 2D and quasi-3D shear deformation theories for free vibration of functionally graded plates on elastic foundations", *Compos. Part B: Eng.*, **159**, 231-247. https://doi.org/10.1016/j.compositesb.2018.09.051.

Zenkour, A., Allam, M. and Radwan, A. (2014), "Effects of transverse shear and normal strains on FG plates resting on elastic foundations under hygro-thermo-mechanical loading", *Int. J. Appl. Mech.*, **6**(05), 1450063. https://doi.org/10.1142/S175882511450063X.